Mixing process in estuaries*

ZHOU Jifu (周济福), LIU Qingquan (刘青泉) and LI Jiachun (李家春)

(Institute of Mechanics, Chinese Academy of Sciences, Beijing 100080, China)

Received April 28, 1999

Abstract A theoretical expression for vertical profile of horizontal velocity in terms of its depth-average is derived based on oscillatory boundary layer theory and estuarine flow characteristics. The derived theoretical profile is then incorporated into a vertical quasi-two-dimensional model, which is proved advantageous in more physical implications and less CPU time demand. To validate the proposed model, the calculated results are compared to the field data in the Yangtze River Estuary, exhibiting good agreement with observations. The proposed quasi-two-dimensional vertical model is used to study mixing process, especially dependence of salinity distribution and salt front strength on runoff and tides in estuaries.

Keywords: estuaries, mixing process, oscillatory boundary layer, salinity.

Recently, people paid more attention to the mixing process in estuaries, where a river enters into open sea and fresh water mixes with salt water. In estuaries, suspended sediment particles flocculate more easily in the salt water environment, thus leading to much larger sediment settling velocity and affecting sediment transport in these areas[1]. It partly accounts for the formation of submerged sand bar, a severe natural obstacle to navigation as well. In addition, intrusion of salt water is an important factor for crop growth, soil improvement and water supply.

There are generally three types of mixing processes corresponding to different estuaries: sharply stratified estuaries or salt-wedge estuaries, partially stratified estuaries and well-mixed estuaries. In a sharply stratified estuary, tidal range is so small and runoff discharge is so large that fresh water runs seaward along the upper layer and salt water intrudes upstream from the lower layer. Mixing only takes place nearby the interface between two layers by entrainment. There have been many researchers who studied this type of mixing, mainly on the dependence of location and geometry of the arrested salt wedge on runoff and tidal discharge, and the interfacial mixing mechanism[2—4]. In a well-mixed estuary where tidal range is large and runoff discharge is small, tidal force causes strong turbulence, and hence results in a vertically uniform salinity profile. The dynamic process can be modeled by one-dimensional hydrodynamic analysis. Han et al.[5] modeled the salt water intrusion in the Qiantangjiang Estuary by using conservative equations of mass, momentum and salinity. As for the partially stratified estuary, such as the Yangtze River Estuary in China, the salinity distribution has displayed distinct three-dimensional characteristics.

Theoretically, a good description for estuarine flow features and transport processes of passive

* Project supported by the National Natural Science Foundation of China (Grant No. 59879025), the National Climbing Project of the Ministry of Science and Technology of China and the Director Foundation of Institute of Mechanics, Chinese Academy of Sciences.

scalars, such as sediment and salinity, can only be obtained by 3D mathematical models. For example, Zhou[6] and Kuang[7] applied the 3D models to the Yangtze River Estuary, giving reasonable explanations for variations of salinity and sediment concentration. However, it is not very easy to get a good insight into the mechanism of passive scalar transport by three-dimensional models with so many physical factors involved. Moreover, the accuracy of three-dimensional analysis is limited by capability of computers available. Therefore, two-dimensional[8] or quasi-3D mathematical models are more practical. For instance, to compute circulation in shallow waters, Jin et al.[9] developed a quasi-3D numerical model composed of two modules, one of which computes the depth-averaged flow, and the other determines the vertical distribution of the flow velocity. Irene et al.[10] proposed a quasi-3D model for suspended sediment transport based on an asymptotic solution of the convection-diffusion equation, in which a flow velocity profile is assumed to have a logarithmic shape. These studies lessen CPU time by simplifying computational method, but lack in physical meaning. At least, it is not reasonable to apply a logarithmic profile to the velocity of oscillatory flow in estuaries at the reversal moment, when upper and bottom fluid flow oppositely. Collins et al.[11] concluded, by analyzing 192 current velocity data sets collected from the intertidal flats of the Loughor Estuary and Swansea Bay (South Wales), that less than 40% of the data sets are logarithmic in character. Hence, the logarithmic velocity profile is not a good assumption for oscillating flow in estuaries.

With an emphasis on the physical processes of estuarine flow, we have analyzed the vertical structure of the flow via oscillatory boundary layer theory and runoff-tide decomposition approach. Then, we propose a model which is capable of predicting salinity advection-diffusion processes rather well and is validated by field measurement in the Yangtze River Estuary. Finally, the proposed model is used to investigate fundamental laws of salt-and-fresh water mixing in estuaries.

1 Vertical structure and estuarine flows

1.1 Estuarine flow characteristics

In an estuarine region, tides force the fluid to oscillate back-and-forth, resulting in periodic variations in flow velocity with tide. In one tidal cycle, there are four particular phases or moments: namely, low water rapid (LWR) with maximal ebb speed, high water rapid (HWR) with maximal tide speed, low water slack (LWS) at which the flow turns from ebb to flood, and high water slack (HWS), the transition instant from flood to ebb. For convenience, we define $u^{\zeta}_{\max}$ and $U_{\max}$ as the top velocity and the depth-integrated one at LWR, respectively, and $u^{\zeta}_{\min}$ and $U_{\min}$ as the top and depth-integrated speeds at HWR, respectively. Around the rapid water instants, the current runs in the way very much similar to a unidirectional flow in a river, owing to the long tidal period, usually 12 or 24 h. While around the slack water instants, flow reversal occurs. The flow is evidently characterized by the upper currents opposite to the lower currents. Runoff, another hydrodynamic factor, superposing on tides, results in a seaward net flux of flow. Therefore, we have $u^{\zeta}_{\max} > -u^{\zeta}_{\min}$ and $U_{\max} > -U_{\min}$. To facilitate analysis, it is necessary to decompose the effect of runoff and tides as follows:

$$U = U_t + U_w, \tag{1}$$

$$u(z) = u_c(z) + u_w(z), \tag{2}$$

where U is the depth-averaged velocity, $u(z)$ the dominant longitudinal, and the along-river current

component at vertical coordinates z; U_w, U_c denote the tide and runoff components of U respectively, and $u_w(z)$, $u_c(z)$ the tide and runoff components of $u(z)$. $u_u(z)$ can be deduced from u_w^ζ, the tide component of the speed at the free surface, via oscillatory boundary layer theory, and $u_c(z)$ can be expressed in terms of u_c^ζ, the runoff component of the speed at the free surface, by using logarithmic law for unidirectional flow velocity, which is accurate enough for engineering purpose, we define

$$u_c^\zeta = \frac{1}{2}[u_{\max}^\zeta + u_{\min}^\zeta], \quad u_w^\zeta = \frac{1}{2}[u_{\max}^\zeta - u_{\min}^\zeta]\cos\phi,$$

in which ϕ is a phase.

According to the logarithmic law of velocity profile, we have

$$u_{\max}^\zeta = U_{\max}\left(1 + \frac{n\sqrt{g}}{\kappa h_{\max}^{1/6}}\right), \quad u_{\min}^\zeta = U_{\min}\left(1 + \frac{n\sqrt{g}}{\kappa h_{\min}^{1/6}}\right),$$

where g is the gravitational acceleration, κ is the von Karman's constant, n is the Manning's roughness coefficient, and $h_{\max}$, $h_{\min}$ are the depths respectively corresponding to $U_{\max}$ and $U_{\min}$.

1.2 Vertical profile of flow velocity

Only based on understanding vertical structure of flow can salinity advection-diffusion processes be described precisely, although horizontal velocity of shallow water flow is nearly uniform. The vertical two-dimensional structure can be delineated by oscillatory boundary layer theory and runoff-tide decomposition, since the characteristic of estuarine flow is similar to that of oscillatory boundary layer as stated above. In this way, $u(z)$, the vertical distribution of horizontal velocity, can be deduced from the time series of U, the depth-averaged velocity. Furthermore, $w(z)$, the distribution of vertical velocity, can be obtained with the help of continuum equation.

1.2.1 Relationship between $u_c(z)$ and u_c^ζ.

Integrating logarithmic formula

$$\frac{u_c(z)}{u_{*c}} = \frac{1}{\kappa}\ln z + c \tag{3}$$

along vertical coordinates yields

$$\frac{U_c}{u_{*c}} = \frac{1}{\kappa}\ln h - \frac{1}{\kappa} + c, \tag{4}$$

in which u_{*c} is the friction velocity of the runoff component of estuarine flow, c is a constant, and h is the water depth. Substitution of h for z into eq. (3) leads to

$$\frac{u_c^\zeta}{u_{*c}} = \frac{1}{\kappa}\ln h + c. \tag{5}$$

Subtracting (3) from (5), we have

$$\frac{u_c^\zeta - u_c(z)}{u_{*c}} = \frac{1}{\kappa}\ln\frac{h}{z}. \tag{6}$$

Subtracting (5) from (4), we have

$$u_c^\zeta = U_c + \frac{u_{*c}}{\kappa}. \tag{7}$$

By the Manning formula we can deduce

$$u_{*c} = n\sqrt{g}U_c/h^{1/6}. \tag{8}$$

Solving the simultaneous eqs. (6)—(8), we obtain the following relationship

$$u_c(z) = u_c^{\zeta}\left(1 - \frac{1}{1 + \frac{\kappa h^{1/6}}{n\sqrt{g}}}\ln\frac{h}{z}\right). \tag{9}$$

1.2.2 Relationship between $u_w(z)$ and u_w^{ζ}. As the reference frame is fixed on the bottom, oscillating water with its top speed as simple harmonic as $u_w^{\zeta} = \frac{1}{2}[u_{\max}^{\zeta} - u_{\min}^{\zeta}]\cos\phi = A\cos\phi$ will cause every layer of fluid in z direction to move back and forth due to the fluid viscosity according to Nielsen[12]. Its velocity distribution can be written as

$$u_w(z) = A\cos\phi - A\exp\left(-\left(\frac{z}{\delta}\right)^p\right)\cos\left(\left(\frac{z}{\delta}\right)^p - \phi\right), \tag{10}$$

in which $\delta = \sqrt{\frac{2\nu}{\omega}}$ is the so-called Stokes length, ν is the kinematic viscosity, ω is the oscillating circular frequency, A is the amplitude, p is a constant which may be 1/3 for turbulent flows, and the phase ϕ is an unknown but should satisfy $U_w = \frac{1}{h}\int_0^h u_w(z)\mathrm{d}z$, where $U_w = U - U_c$, and U_c can be obtained by solving (7) and (8) simultaneously. Substitution of (10) and integration lead to

$$\begin{aligned} U_w &= \sqrt{(A+\alpha)^2 + \beta^2}\sin(\phi + \psi), \\ \phi &= \arcsin\frac{U_w}{\sqrt{(A+\alpha)^2 + \beta^2}} - \psi, \end{aligned} \tag{11}$$

in which $\psi = \arctan\frac{A+\alpha}{\beta}$,

$$\alpha = \frac{A\delta}{2ph}\left\{\exp\left(-\left(\frac{h}{\delta}\right)^p\right)\left[\left(\frac{h}{\delta}\right)^p + 1\right]\left[\left(\left(\frac{h}{\delta}\right)^p - 1\right)\cos\left(\frac{h}{\delta}\right)^p - \left(\left(\frac{h}{\delta}\right)^p + 1\right)\sin\left(\frac{h}{\delta}\right)^p\right] + 1\right\},$$

$$\beta = \frac{A\delta}{2ph}\left\{\exp\left(-\left(\frac{h}{\delta}\right)^p\right)\left[\left(\frac{h}{\delta}\right)^p + 1\right]\left[\left(\left(\frac{h}{\delta}\right)^p + 1\right)\cos\left(\frac{h}{\delta}\right)^p + \left(\left(\frac{h}{\delta}\right)^p - 1\right)\sin\left(\frac{h}{\delta}\right)^p\right] - 1\right\}.$$

Eqs. (9)—(11) establish the relationship between $u(z)$ and U, by which the two-dimensional flow field can be obtained based on one-dimensional velocity field rather than solving the two-dimensional momentum equations directly.

2 Vertical two-dimensional model and its validation

2.1 Governing equations

One-dimensional continuum equation in shallow water is

$$\frac{\partial\zeta}{\partial t} + \frac{\partial Uh}{\partial x} = 0. \tag{12}$$

And the momentum equation looks like

$$\frac{\partial U}{\partial t} + U\frac{\partial U}{\partial x} = -g\frac{\partial\zeta}{\partial x} - \frac{gh}{\rho}\frac{\partial\rho}{\partial x} - g\frac{|U|U}{C^2h}. \tag{13}$$

The state equation is written as

$$\rho = \rho_0 + \eta s. \tag{14}$$

In addition, the vertical two-dimensional continuum equation takes the form of

$$\frac{\partial u}{\partial x} + \frac{\partial w}{\partial z} = 0, \tag{15}$$

and the vertical two-dimensional advection-diffusion equation of salinity is

$$\frac{\partial s}{\partial t} + \frac{\partial us}{\partial x} + \frac{\partial ws}{\partial z} = \frac{\partial}{\partial x}\left(D_x \frac{\partial s}{\partial x} \right) + \frac{\partial}{\partial z}\left(D_z \frac{\partial s}{\partial z} \right). \tag{16}$$

In the above equations, t is the time, x, z are the horizontal (seaward) and vertical (upward) coordinates, respectively, ζ is the water level, h is the depth, U is the vertically mean velocity, g is the gravitational acceleration, C is the Chezy coefficient, ρ, ρ_0 are densities of salty and fresh water respectively, $\bar{\rho}$ is the depth-averaged density, s is the salinity, η is a constant which approximates 0.000 7 provided s is measured in ‰, u, w respectively denote x-component and z-component of the flow velocity, and D_x and D_z are horizontal and vertical turbulent diffusivity.

2.2 Solving steps and methods

The steps to solve the above equations are as follows. First, solving eqs. (12)—(14) simultaneously yields the time series of mean speed U and water level ζ in a tidal cycle. Secondly, $u(z)$ is obtained via eqs. (9)—(11). Thirdly, $w(z)$ is deduced from continuum eq. (15). And finally, the salinity advection-diffusion eq. (16) is solvable. By the above steps salinity distributing in the vertical plane is obtainable. However, iterations are needed due to the unknown s in the state equation.

Numerical method must be used to solve eqs. (12) and (13) for the nonlinearity. Here, we adopt Preissmann implicit finite difference scheme, commonly used for its advantages of good stability and less CPU time. Eq. (16) is discretized by up-wind difference scheme and ADI method. TDMA approach is introduced to solve the discrete equation system.

2.3 Validation of the model

Measurements in the North Channel waterway of the Yangtze River Estuary are used for validation. The measurements include hourly tide levels on September 3, 4 and 5, 1989 at the gauging stations of Hengsha, Middle of North Channel, 18 km downstream from Hengsha, and Jiuduandong, 40 km downstream from Hengsha, and salinity data at SN2, SN3 and SN4, respectively situated at 8, 12 and 16 km downstream from Hengsha station. The simulated domain is meshed with horizontal space step $\Delta x = 2$ km, 20 grid points, and vertical divisions of 10 layers, 11 grid points (including those at the bottom and the free surface). The time step is $\Delta t =$ 60 s and the roughness coefficient $n = 0.01$. Taking Hengsha station as the upstream boundary and Jiuduandong as the downstream boundary, with a 24-h time series of tide levels during 6:00 September 4—6:00 September 5 as the boundary conditions and $\zeta(x, 0) = 0$ and $U(x, z, 0) = 0$ as the initial conditions, we simulate the time series of water level at Middle of North Channel station, which is compared with the measurement in fig. 1, showing good agreement. Fig. 2 depicts the calculated flow field in vertical plane around HWR and LWR. Vectors in the figures demonstrate that horizontal component of the

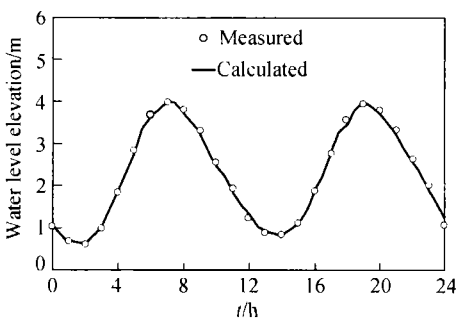

Fig. 1. Time series of water level at Middle of North Channel.

velocity is much greater than the vertical component. These patterns is implied by dimensional analysis. If the scales of horizontal and vertical components of the flow velocity are characterized by U and W, respectively, and the length scales in horizontal and vertical directions are denoted by L and H, respecively. $W = UH/L$ holds from the continuity equation (15). In the present case, $H = 10$ m, $L = 40\,000$ m, and hence $W = 2.5 \times 10^{-4}\,U$, suggesting that the calculated flow field reveals the real flow patterns approximately.

As for salinity validation, the downstream boundary is placed at the site of SN4 owing to the lack of salinity data at Jiuduandong station, where water levels, as boundary conditions, are obtained from the water level validation. Salinity at Hengsha as the upstream boundary can be taken as zero because Hengsha station is situated approximately at the limit section which divides salt and fresh water[13]. According to Kuang[7], horizontal diffusivity $D_x = 500$ m^2/s, and vertical diffusivity has the form

$$D_z = \begin{cases} \kappa u_* z\left(1 - \dfrac{z}{h}\right), & \dfrac{z}{h} < 0.5, \\ \dfrac{1}{4}\kappa u_* h, & \dfrac{z}{h} \geqslant 0.5. \end{cases}$$

Here u_* is the friction velocity of the mean flow. Initial salinity field $s(x, z, 0) = 0$ leads to the stable results only after a few tidal cycles. Fig. 3 compares the calculated salinity time series at the site of SN3 with the measured ones at six different heights of 0.0, 0.2, 0.4, 0.6, 0.8 and 1.0 h. The agreements are rather well, i.e. they are within the permitted errors for engineering purpose.

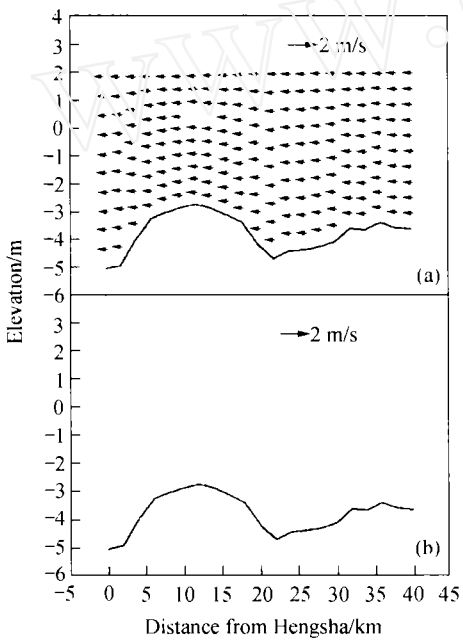

Fig. 2. Flow fields around instants of HWR (a) and LWR (b) in North Channel waterway.

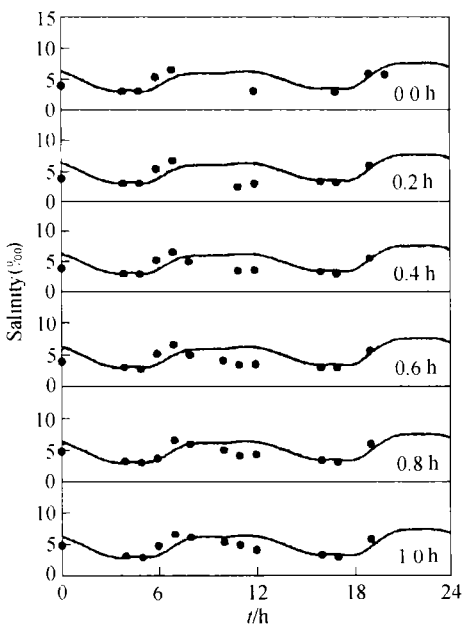

Fig. 3. Time series of salinity at the site of SN3.

3 Influences of runoff and tides on the salt-and-fresh water mixing

Usually, mixing processes in estuaries are very complicated due to the coupled interactions of

different dynamic factors and irregular topography. For simplicity, a plane bottom is assumed to facilitate analyzing the influences of runoff and tides on the mixing processes. The adopted parameters are referred to those of North Channel waterway of the Yangtze River Estuary. For example, the depth is taken as 10 m below theoretical datum plane. The hydrological factors are given in table 1.

Table 1 Parameters for the studied cases

Case label	Conditions		N	$\Delta s/\Delta x/\mathrm{km}^{-1}$	
	te/m	uc/m·s^{-1}		HWS	LWS
a	2.0	0.1	0.13	0.48	0.73
b	1.0	0.1	0.18	0.61	0.86
c	0.5	0.1	0.22	0.69	1.03
d	0.5	0.2	0.40	1.09	2.11
e	0.5	0.3	0.57	1.50	3.10

In table 1, te denotes the amplitude of tide level, half of the tidal range, uc stands for the runoff component of velocity at the upstream boundary, and N, called mixing index, is defined as the ratio of runoff volume to the flood volume during tides, expressing the relative strength of runoff and tides.

3.1 Longitudinal distribution of mean salinity

Variations of salinity with runoff and tides can be obtained by case studies (see fig. 4). Comparisons between cases a—c and between cases c—e reveal the variations of salinity with tides and runoff respectively. Fig. 4 suggests that longitudinal mean salinity distribution is dependent on phase, tidal range and runoff discharge. The gradient is the smallest for the most upstream salt water intrusion at HWS, while it is the greatest for the most downstream salt water intrusion at LWS. And it is between these two values at any other moments. At a given phase, the gradient decreases with increasing tidal range or hydrodynamic tidal force, if runoff discharge remains unchanged. When $te = 2.0$ m, $uc = 0.1$ m/s, the longitudinal salinity profile is approximately linear. If tidal range remains the same, an increase of the runoff discharge causes large salinity gradient, the longitudinal profile deviating from linear one. In fact, we may as well introduce one variable, the mixing index, to explain the variation of longitudinal salinity distribution at a given phase with tides and runoff. For cases a—e, the degree of mixing becomes weaker gradually, its index increases, and salinity gradient grows correspondingly. When the index takes the value of 0.13, the longitudinal salinity profile approximates to a linear one.

3.2 Variations of salt front

The "front" concept was early used in meteorology, representing the interface between two air masses with different temperatures. This concept has been introduced into oceanography to describe the interface between two water masses with different temperatures or densities, where the gradient of every hydrological quantity (such as salinity and density) is large. Nearby the front, salinity favors the flocculation of sediment particles, and the circulation caused by density difference concentrates the suspended sediment. All these effects result in the formation of "turbidity maximum" in an estuary.

The salt front intensity can be quantified by the longitudinal salinity gradient, $\frac{\Delta s}{\Delta x}$. In the table

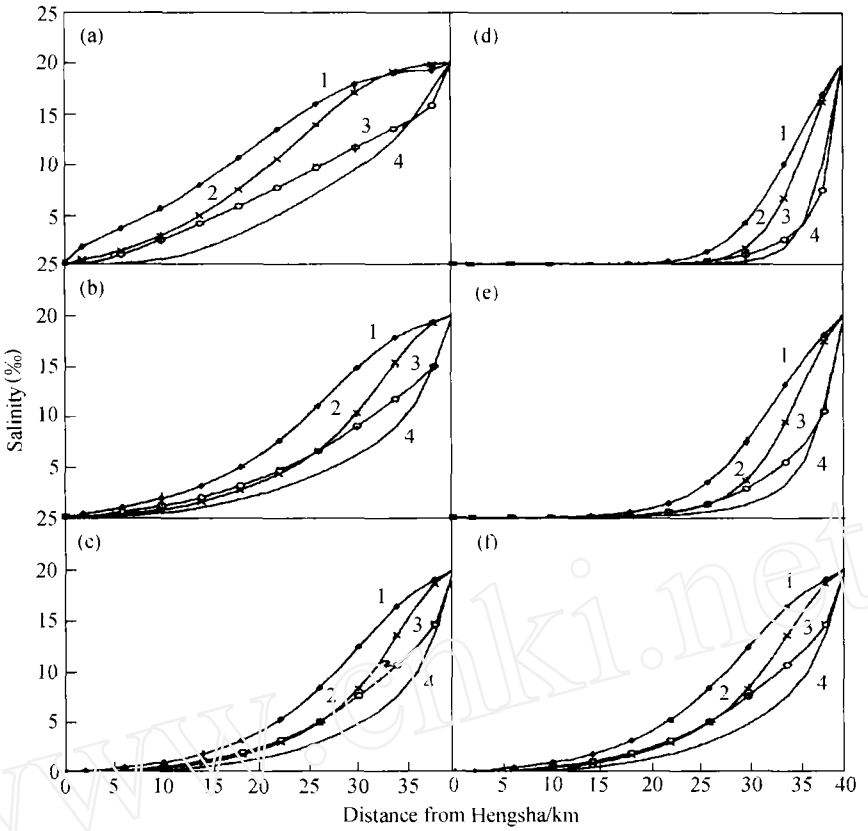

Fig. 4. Variations of longitudinal distribution of mean salinity with runoff and tides. 1, HWS; 2, HWR; 3, LWR; 4, LWS. (a) Case a: $te = 2.0$, $uc = 0.1$; (b) case b: $te = 1.0$, $uc = 0.1$; (c) case c: $te = 0.5$, $uc = 0.1$; (d) case e: $te = 0.5$, $uc = 0.3$; (e) case d: $te = 0.5$, $uc = 0.2$; (f) case c: $te = 0.5$, $uc = 0.1$.

of studied cases the mean salt front intensities at HWS and LWS are listed. The figures show that $\frac{\Delta s}{\Delta x}$ increases with N, namely, the salt front becomes more intense with runoff discharge increasing and tidal range decreasing. Thus it can be inferred that the salt front intensity in flood season is greater than that in dry season. On the other hand, the salt front intensity on ebb is greater than that on flood, owing to the seaward movement of the salt front forced by runoff on ebb and the upstream movement of the salt front forced by tide on flood. These statements are as well demonstrated by fig. 4. Fig. 5 plots $\frac{\Delta s}{\Delta x}$ against N, showing approximately linear increases of salt front intensities with mixing indices, with different slopes at different phases (the slope turns from its minimum at HWS to the maximum at LWS).

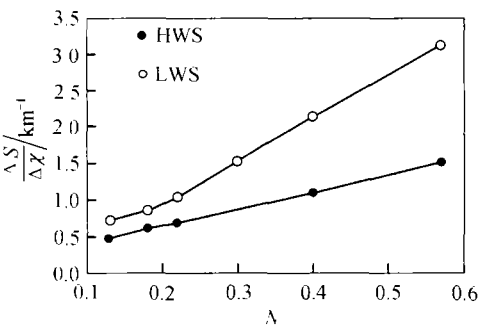

Fig. 5 Relationship of salt front intensity and mixing index.

Field measurements indicate that a salt front with

the greatest longitudinal salinity gradient exists in an estuary all the year round. Its intensity and position are phase-, runoff- and tide-dependent. This is indicated in fig. 4. At HWS instant, the greatest salinity gradients of cases a—e are 0.70, 0.94, 1.00, 1.37 and 1.78 km^{-1}, respectively. The fronts are located at some 20, 25, 28, 32 and 36 km downstream from Hengsha station, with the position displacement approximate 16 km.

3.3 Salinity distributions in the vertical plane

Salinity contours in the vertical plane (see fig. 6) describe the patterns of salinity distribution both in longitudinal and vertical directions, which show different characteristics related to different combinations of hydrological factors, and periodic variations for a given combination of hydrological factors. In fig. 6(a)—(d) are plotted the contours of case b (te = 1.0 m, uc = 0.1 m/s) at slack water and rapid water phases, which once again depict the characteristics of longitudinal mean salinity distribution shown in fig. 4, e. g. the salt front intrudes most upstream at HWS for tide effects, and is pushed to the most downstream end at LWS by runoff force. Meanwhile, a rudimentary salt-wedge can be seen from the figures, which results from density flow. On the other hand, in the vicinity of the upstream end, to which salt water cannot reach, and the downstream end, where there is little fresh water, salinity distributed uniformly in vertical direction. Therefore, the vertical salinity gradient experiences a small-to-great-to-small variation, suggesting uniform vertical salinity profiles at the two ends and non-uniform ones in the middle area.

Figure 6(d)—(f) compare the salinity contours of different tidal ranges, 0.5, 1.0 and 2.0 m, with the same runoff discharge. It can be seen that the salt front approaches more upstream with increasing tidal force when runoff discharge remains unchanged, with a 5-km shift of front locations. Likewise, a comparison of the salinity contours of different uc values, 0.1, 0.2 and 0.3 m/s, with a given tidal range is made between fig. 6(f), (g) and (h), suggesting that an increase of runoff discharge constrains the upstream intrusion of the salt water and makes the salt front move seaward, with a 15-km shift of front positions. Therefore, effects of runoff and tides make the salt front oscillate downstream and upstream respectively, the former effect being more apparent.

4 Concluding remarks

Based on the physics of estuarine flow, we have derived the vertical velocity profile of an oscillatory flow via oscillatory boundary layer theory and runoff-tide decomposition approach. And we have proposed a quasi-2D model for flow and salinity predictions, which is validated by the field measurements in North Channel waterway of the Yangtze River Estuary.

The proposed model is used to study salt-and-fresh water mixing processes in estuaries. General conclusions are drawn as follows: Longitudinal salinity distributions vary with the relative dominance of runoff or tides. When the mixing index approaches to 0.1, they are linearly distributed. In addition, the distribution gradients are phase dependent, taking the smallest value at HWS and the greatest one at LWS. As for the vertical salinity distributions, the gradients experience small-to-great-to-small variations. A salt-wedge can be found at the downstream end. The salt front moves seaward with increasing runoff discharge, and shifts upstream with increasing tide forces. The mean salt front intensity approximately varies with the mixing index linearly.

The model sets a foundation for further studying sediment transport in estuaries. As compared

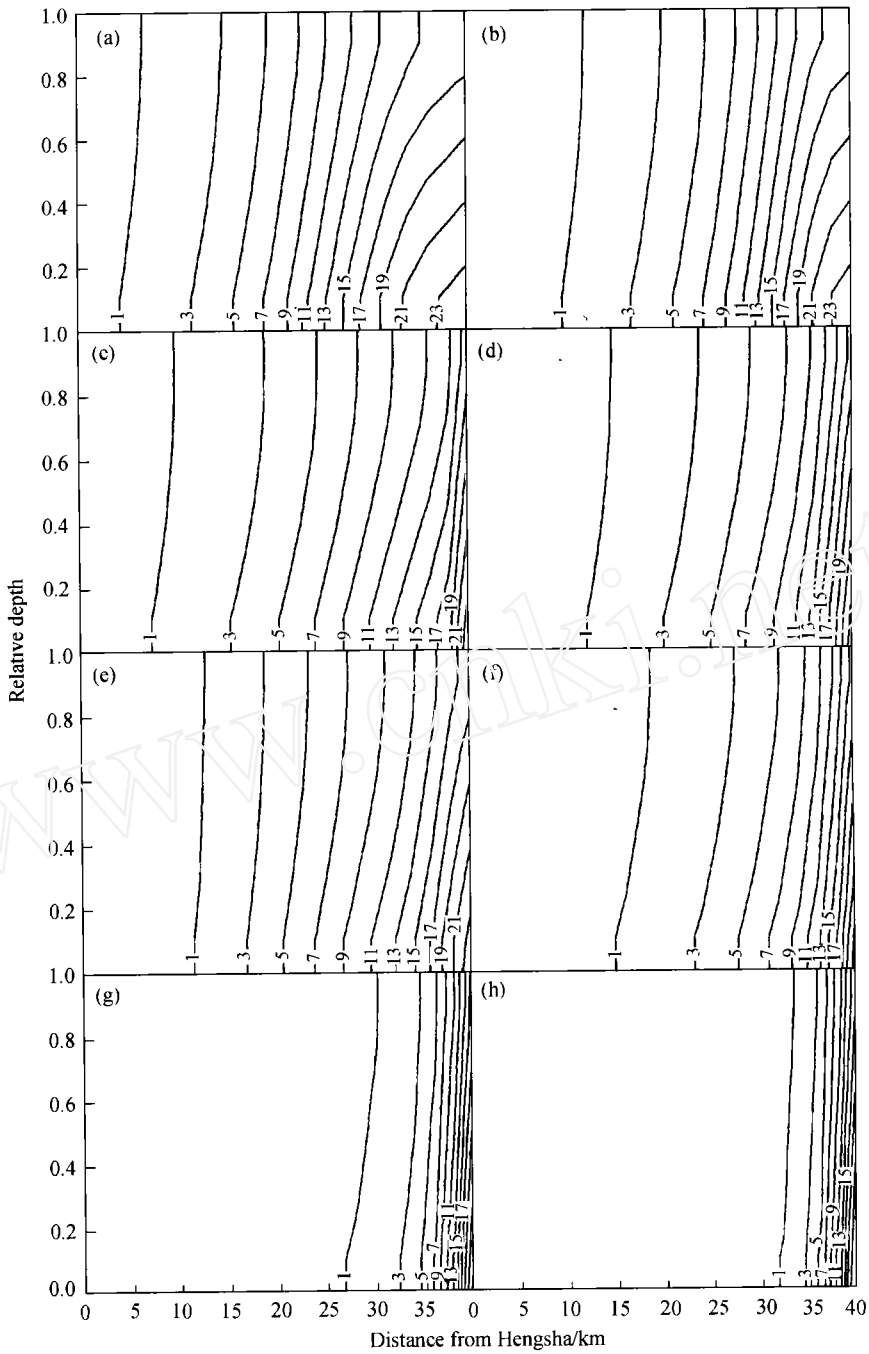

Fig. 6. Variations of salinity contours with time, runoff and tides.

with other simplified mathematical models, it is advantageous in more apparent physical implications and less CPU time. However, the model is not kept valid in some local areas where topography changes abruptly due to the deviations of flow from oscillatory boundary layer. Also, for the strongly stratified estuaries, the model again leads to some errors, since the flow is no longer one-dimensional

owing to the large vertical salinity gradient.

References

1 Mao, Z., A study on salt fronts in the Changjiang River Estuary, *Oceanologia et Limnologia Sinica* (in Chinese), 1995, 26(5): 643.

2 Grubert, J. P., Interfacial mixing in stratified channel flows, *J. Hydr. Div. ASCE*, 1989, 115(7): 887.

3 Grubert, J. P., Interfacial mixing in estuaries and fjords, *J. Hydr. Engrg.*, 1990, 116(2): 176.

4 Kurup, G. R., Hamilton, D. P., Patterson, J. C., Modeling the effect of seasonal flow variations on the position of salt wedge in a microtidal estuary, *Estuarine, Coastal and Shelf Science*, 1998, 47: 191.

5 Han, Z., Shao, Y., Lu, X. et al., Numerical and experimental predictions of salt water intrusion in estuaries, in *Proceedings of 6th Conference on Computational Fluid Dynamics* (in Chinese), Beijing: Science Press, 1992: 331.

6 Zhou, H., A study on characteristics of maximum turbidity zone in the Changjiang River Estuary and three-dimensinal numerical modeling of flow and sediment transport, *Doctoral Thesis* (in Chinese), Nanjing: Hohai University, 1992.

7 Kuang, C., A study on changes of mouth bar and suspended sediment settlement in the Changjiang River Estuary and mathematical model for flow and transport of salinity and sediment, *Doctoral Thesis* (in Chinese), Nanjing: Nanjing Institute of Water Conservancy, 1993.

8 Bloss, S., Lehfeldt, R., Patterson, J. C., Modeling turbulent transport in stratified estuary, *J. Hydr. Engin., ASCE*, 1998, 114(9): 1115.

9 Jin, X., Krennburg, C., Quasi-3D numerical modeling of shallow-water circulation, *Journal of Hydraulic Engineering*, 1993, 119(4): 458.

10 Irene, K., Jan, S. R., Quasi-3D modeling of suspended sediment transport by currents and waves, *Coastal Engineering*, 1992, 18: 83.

11 Collins, M. B., Ke, X., Cao, S., Tidally-induced flow structure over intertidal flats, *Estuarine, Coastal and Shelf Science*, 1998, 46: 233.

12 Nielsen, P., Coastal bottom boundary layers and sediment transport, *Advanced Series on Ocean Engineering*, Vol. 4, Printed in Singapore by JBW Printers & Binders Pte. Ltd., 1992.

13 Wang, Y., Zhang, Z., Hydrochemical characteristics and clay minerals of suspended sediment in South Channel, Changjiang Estuary, *Marine Science Bulletin* (in Chinese), 1995, 14(3): 106.